

ON THE DETECTABILITY OF ULTRA-COMPACT BINARY PULSAR SYSTEMS

NIHAN POL

Department of Physics and Astronomy, West Virginia University, Morgantown, WV 26506-6315
 Center for Gravitational Waves and Cosmology, West Virginia University, Chestnut Ridge Research Building, Morgantown, West Virginia 26505 and

Department of Physics and Astronomy, Vanderbilt University, 2301 Vanderbilt Place, Nashville, TN 37235, USA

MAURA McLAUGHLIN, DUNCAN R. LORIMER, AND NATHAN GARVER-DANIELS

Department of Physics and Astronomy, West Virginia University, Morgantown, WV 26506-6315 and
 Center for Gravitational Waves and Cosmology, West Virginia University, Chestnut Ridge Research Building, Morgantown, West Virginia 26505

Draft version March 17, 2024

ABSTRACT

Using neural networks, we integrate the ability to account for Doppler smearing due to a pulsar’s orbital motion with the pulsar population synthesis package PSRPOP to develop accurate modeling of the observed binary pulsar population. As a first application, we show that binary neutron star systems where the two components have highly unequal mass are, on average, easier to detect than systems which are symmetric in mass. We then investigate the population of ultra-compact ($1.5 \text{ min} \leq P_b \leq 15 \text{ min}$) neutron star–white dwarf (NS–WD) and double neutron star (DNS) systems which are promising sources for the Laser Interferometer Space Antenna gravitational-wave detector. Given the non-detection of these systems in radio surveys thus far, we estimate a 95% confidence upper limit of ~ 1450 and ~ 1100 ultra-compact NS–WD and DNS systems in the Milky Way that are beaming towards the Earth respectively. We also show that using survey integration times in the range 20 s to 200 s with time-domain resampling will maximize the signal-to-noise ratio as well as the probability of detection of these ultra-compact binary systems. Among all the large scale radio pulsar surveys, those that are currently being carried out at the Arecibo radio telescope have $\sim 50\text{--}80\%$ chance of detecting at least one of these systems using current integration times and $\sim 80\text{--}95\%$ using optimal integration times in the next several years.

Subject headings: pulsars: general — pulsars: binary — gravitational waves

1. INTRODUCTION

The era of multi-messenger astronomy was ushered in with GW170817, a detection of gravitational waves (GWs) emitted by the merger of two neutron stars using the Laser Interferometer Gravitational-wave Observatory (LIGO, Harry & LIGO Scientific Collaboration 2010) and Virgo (Accadia et al. 2012) detectors (Abbott et al. 2017a) as well as across the electromagnetic spectrum by a range of ground and space-based telescopes (Abbott et al. 2017b). While LIGO–Virgo has made another confirmed detection of a double neutron star (DNS) merger event (Abbott et al. 2020) and released alerts for a few more potential DNS mergers, these are relatively rare cataclysmic events. On the other hand, the Laser Interferometer Space Antenna (LISA, Amaro-Seoane et al. 2017) is a space-based GW detector which is sensitive to compact objects in binary systems emitting GWs at frequencies between $0.1 \text{ mHz} \lesssim f_{\text{GW}} \lesssim 100 \text{ mHz}$. Given the abundance of binaries consisting of compact objects as well as their non-cataclysmic nature, these systems provide rich potential for long-term multi-messenger science.

The strongest sources for LISA are Galactic ultra-compact binary (UCB) systems, which are binary systems with stellar-mass components and orbital periods $P_b < 15 \text{ min}$. These UCB systems can consist of any combination of white dwarf, neutron star or black holes, with the most common source ($\sim 10^7$ in the Galaxy)

being double white dwarf (DWD) binaries (Nelemans et al. 2001a,b). However, population synthesis simulations have shown that LISA should also detect a few tens of ultra-compact double neutron star (DNS) and neutron star–white dwarf (NS–WD) systems (Andrews et al. 2020; Lau et al. 2020). UCB systems are “verification binaries” for LISA, i.e. they should be detectable within weeks of LISA beginning operations. Verification binaries for DWD systems have already been identified in the electromagnetic (EM) band using optical surveys (Brown et al. 2010; Kilic et al. 2010; Napiwotzki et al. 2004). However, no verification binary consisting of a neutron star has been detected yet. The most promising DNS system for detection by LISA is the Double Pulsar system, J0737–3039 (Burgay et al. 2005), but this system will only accumulate a signal-to-noise ratio (S/N) of ~ 3 over the planned 4-yr LISA mission.

Joint, multi-messenger observations of these UCB systems can provide significantly more information than observations in the EM or GW bands alone. As shown by Shah et al. (2012), measuring the inclination of an UCB system through EM observations can improve the constraint on the GW amplitude of that system by a factor as large as six. In addition, knowing the sky position of an UCB system can improve the GW parameter estimation by a factor of two (Shah et al. 2013). Additionally, for DNS systems, joint EM and GW observations can constrain the mass-radius relation to within $\approx 0.2\%$

(Thrane et al. 2020). Thus, it is important to find as many UCB systems as possible before LISA is launched in the 2030s to maximize the scientific potential of the mission.

In the EM band, neutron star binaries are discovered by searching for pulsars, which are rapidly rotating neutron stars emitting beamed emission at radio wavelengths. So far, 185 pulsars have been discovered in binary systems with a white dwarf companion, while 20 pulsars have been discovered in binary systems with another neutron star (for an up-to-date list, see the ATNF pulsar catalog¹, Manchester et al. 2005). The shortest orbital period for a pulsar–WD binary is ~ 2 hours (PSR J1518+0204C, Hessels et al. 2007; Pallanca et al. 2014), while for DNS systems the shortest orbital period is ~ 1.8 hours (J1946+2052, Stovall et al. 2018). Henceforth in this paper, we assume that the binary system contains a pulsar whenever we refer to ultra-compact NS–WD or DNS systems.

The limiting factor in detecting UCB systems in radio-wavelength surveys is the Doppler smearing of the pulsar emission due to its orbital motion (Johnston & Kulkarni 1991a) as it causes a reduction in the S/N with which the pulsar is detected. This Doppler smearing is quantified using the orbital degradation factor (Johnston & Kulkarni 1991a), which can take values between 0 and 1, and lower values of the orbital degradation factor signify higher Doppler smearing and thus a larger reduction in S/N for the pulsar. The orbital degradation factor depends on, among other things, the orbital period of the binary system and is smaller for systems with small orbital periods. Thus, UCB systems, with their extremely small orbital periods, are difficult to detect in normal radio pulsar surveys.

To improve sensitivity to pulsars in binary systems, where the apparent pulse period can change significantly during the observation due to the Doppler effect, acceleration and jerk search techniques are employed in radio pulsar surveys (see Lorimer & Kramer 2004, for a review of implementation techniques). Acceleration searches have now been widely implemented in the search pipelines for almost all large radio pulsar surveys (for example, Eatough et al. 2013), while jerk searches are only recently being implemented (Andersen & Ransom 2018) due to the technique being significantly more computationally expensive than acceleration searches. The effect of the acceleration search technique on the S/N of the pulsar was quantified in Johnston & Kulkarni (1991a) for circular binaries, while Bagchi et al. (2013) expanded their work to include eccentric systems as well as the effect of jerk search techniques.

While these techniques have been well known in the literature, they have never been fully incorporated into pulsar population synthesis simulations. While Bagchi et al. (2013) did provide software to compute the orbital degradation factors, the calculations (much like the search techniques themselves) are time-intensive and thus not optimized for inclusion in large scale population synthesis analysis such as PSRPOPpy (Bates et al. 2014). As a result, there has not been any significant modeling of the observed binary pulsar populations.

In this work, we develop a computationally efficient

framework to calculate the orbital degradation factor using the software provided by Bagchi et al. (2013). To do this, we integrate the orbital degradation factor into PSRPOPpy (Sec. 2), a pulsar population synthesis package designed to model the observed pulsar population discovered in multiple radio surveys at different radio frequencies (Bates et al. 2014). We use this to place upper limits on the population of ultra-compact NS–WD and DNS systems in the Milky Way given that we have not yet detected any such system (Sec. 3) and calculate the probability for any of the current large pulsar surveys to detect these UCB systems. Finally in Sec. 4, we calculate a range of optimum integration times that will maximize the S/N for UCB systems, thereby increasing the probability of detection of these systems in radio surveys.

2. INTEGRATING ORBITAL DEGRADATION FACTOR INTO PSRPOPpy

We use the framework developed in Bagchi et al. (2013) to calculate the orbital degradation factor for a binary system. The orbital degradation factor, γ , can take values between $0 \leq \gamma \leq 1$ and when calculated at the harmonic, m , depends on the mass of the pulsar, m_1 , and the companion, m_2 , the orbital period, P_b , eccentricity, e , inclination, i , and angle of periastron passage, ω_p , as well as the spin period of the pulsar, P_s , and the integration time of the survey, t_{obs} (Johnston & Kulkarni 1991a). The orbital degradation factor can be calculated for the case of a normal pulsar search (γ_1) as well as pulsar searches which apply acceleration (γ_2) and jerk (γ_3) search techniques. The radiometer S/N for the pulsar in the binary system is reduced by a factor of γ_i^2 , where $i = [1, 2, 3]$ depending on the type of search technique. A lower orbital degradation factor implies a lower recovered S/N for the pulsar in the binary system due to Doppler smearing of the its signal from its orbital motion. We assume all modern pulsar surveys use acceleration search techniques and present results based on γ_2 in this work.

The software to calculate the orbital degradation factor that was provided with Bagchi et al. (2013) is computationally inefficient for use in large scale population synthesis simulations. To solve this problem, we used this software as a data generator to train a simple neural network to calculate the orbital degradation factor for a given binary system.

2.1. Data standardization

The neural network takes the parameters described above as an input to calculate the orbital degradation factor. The range of training values for each of the input parameters are shown in Table 1. These values are chosen to span the expected range of values for the population. We limit the harmonic, m , to a maximum value of 5, since the power in larger harmonics is relatively negligible for binary systems (Bagchi et al. 2013). We also allow the companion mass, m_2 , to vary up to $10^9 M_\odot$ to allow simulation of pulsars orbiting the Milky Way’s central supermassive black hole, Sgr A*, which has a mass $\sim 10^6 M_\odot$, as well as an even more massive hypothetical supermassive black hole. Since some of the input parameters can span multiple orders of magnitude, it is necessary to normalize the data to ease the training of

¹ <https://www.atnf.csiro.au/research/pulsar/psrcat/>

TABLE 1

IN THIS TABLE, WE SHOW THE RANGE OF VALUES OF THE INPUT PARAMETERS FOR WHICH THE NEURAL NETWORK PRESENTED IN THIS WORK IS TRAINED.

Name of parameter	units	Minimum	Maximum
Harmonic, m	—	1	5
Survey integration time, t_{obs}	seconds	1	5×10^3
Mass of pulsar, m_1	M_{\odot}	1	2.4
Mass of companion, m_2	M_{\odot}	0.2	10^9
Spin period of pulsar, P_s	seconds	10^{-3}	5
Inclination of binary system, i	degrees	0°	90°
Angle of periastron passage, ω_p	degrees	0°	360°
Eccentricity, e	—	0	0.9
Orbital period, P_b	days	10^{-3}	10^3

the neural network. Thus, we first take the logarithm of the parameters t_{obs} , m_1 , m_2 , P_s , and P_b so that they have a dynamic range similar to the other input parameters. Next we normalize all of the input parameters such that they fall in the range between ± 1 .

2.2. Network architecture

We use KERAS (Chollet et al. 2015) with the TENSORFLOW (Abadi et al. 2015) backend to develop our neural network model. The neural network consists of five layers, with the input layer having 9 nodes (equal to number of inputs), three “hidden” layers containing 32 nodes, and the final, output layer consisting of a single node. We use the “swish” activation function (Ramachandran et al. 2017) for the hidden layers, while the output layer used a linear activation function. Since we assume that all surveys use the acceleration search technique, we will describe the training and performance of the neural network that models the acceleration search technique below (i.e. γ_2). However, the results are similar for the neural networks modeling the other search technique.

2.3. Training the neural network

We generate 69566 combinations of the parameters described in Table 1 and calculate the corresponding γ_2 values using the software provided with Bagchi et al. (2013). We take care to ensure that the training dataset spans the entire range of parameters described in Table 1. We extract 5% of this as a test dataset using which we can quantify the accuracy of the trained neural network. The remaining data have another 5% reserved to be used as the validation dataset.

During training, the neural network uses the input parameters to predict the orbital degradation factor (referred to as the prediction) which is then compared to the orbital degradation factor calculated using the analytical calculation (referred to as the label) in Bagchi et al. (2013). We use the mean absolute percentage error,

$$\text{MAPE} = \left\langle 100 \times \frac{|\text{prediction} - \text{label}|}{\text{label}} \right\rangle \quad (1)$$

as the loss function for our neural network. We use the Adaptive Moment (“ada”, Kingma & Ba 2014) technique to optimize the learning for the neural networks and we stop training the neural network once the MAPE has stopped improving for the validation dataset.

The accuracy of this trained neural network can be calculated by evaluating its performance on the test dataset.

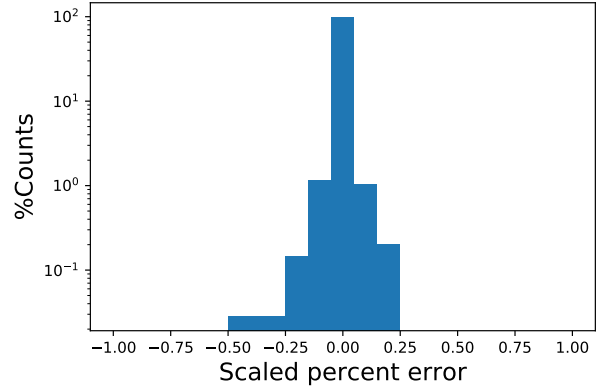


FIG. 1.— The distribution of the scaled percent error (Eq. 2) for the γ_2 neural network evaluated on the training dataset.

We quantify the accuracy of the neural network through the distribution of the scaled percent error,

$$\text{SPE} = 100 \times \frac{\text{prediction} - \text{label}}{\text{label}}, \quad (2)$$

which is shown in Fig. 1. As we can see, 97.44% of the predictions made by the neural network have an error of $\leq 5\%$ compared to the values predicted using the analytic solution from Bagchi et al. (2013), while there are almost no values with an error $\gtrsim 25\%$.

The orbital degradation factor computation using the neural network framework is faster by a factor of 10^4 compared to the same computation using the software provided by Bagchi et al. (2013). This demonstrates the suitability of the former for large scale population synthesis simulations. In addition, the inherent parallelism of the neural network framework allows it to compute multiple orbital degradation factors in a single pass while the software provided with Bagchi et al. (2013) was limited to a single computation. This provides an additional significant improvement in the computational efficiency of the neural network framework.

We can directly compare the results produced by the trained neural network to those published in Bagchi et al. (2013) by reproducing the figures from that work. As an example, in Fig. 2, we compare the results presented in Fig. 9(b) of Bagchi et al. (2013) with those produced by our neural network. As we can see, the results produced by the two methods are identical, which is another confirmation of the accuracy of our neural network.

2.4. Integration with PSRPOPpy

The orbital degradation factor calculated with the neural network can be directly integrated into PSRPOPpy for modeling the different types of binary pulsar populations. We add the ability for PSRPOPpy to generate orbital parameters for a synthetic pulsar² which are used to compute the orbital degradation factor. PSRPOPpy calculates the S/N for a pulsar using the radiometer equation (Lorimer & Kramer 2004), which can be directly scaled by γ^2 (Bagchi et al. 2013) to get the S/N for the same pulsar if it were in a binary.

² <https://github.com/NihanPol/PSrPopPy2>

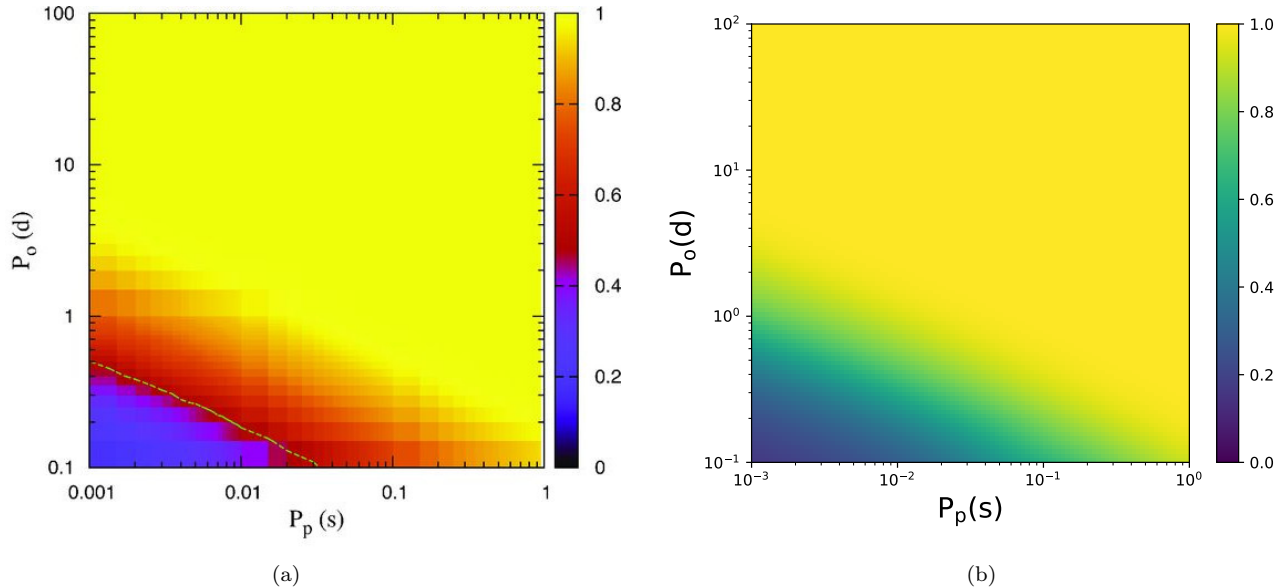


FIG. 2.— We directly compare the results from Fig. 9(b) in Bagchi et al. (2013) (panel (a)) to the γ_2 neural network trained in this work (panel (b)). In both plots, the X-axis shows the spin period of the pulsar, the Y-axis shows the orbital period of the BNS system and the colorbar represents the orbital degradation factor. As we can see, the two methods produce identical results for the orbital degradation factor, γ_2 .

2.5. Selection bias against asymmetric mass DNS systems

As an application of the orbital degradation factor, we investigate whether it is easier to detect a DNS system that is symmetric in mass as compared to the same system if it were asymmetric in mass. The question depends only on how the orbital degradation factor depends on the mass ratio of the binary system. To investigate this, we perform a Monte Carlo simulation where we randomly draw samples from the distributions for all the input parameters to the orbital degradation factor. The majority of the observed sample of NS–WD and DNS systems have spin periods less than ~ 100 ms (Manchester et al. 2005). Similarly, the majority of the observed NS–WD systems have orbital periods less than ~ 50 days, while the majority of the observed DNS systems have orbital periods less than ~ 10 days (Manchester et al. 2005). To correspond to the observed sample, we restrict the range of spin and orbital periods for the pulsars to be in the range $1 \text{ ms} < P_s < 100 \text{ ms}$ and $10^{-3} \text{ days} < P_b < 50 \text{ days}$ respectively. Other parameters are allowed to vary across their full range as listed in Table 1. However, in place of using the companion mass directly, we instead define a new parameter, the mass ratio, $q = m_1/m_2$. We define symmetric systems as those having $0.9 \leq q \leq 1.0$ and asymmetric systems as $0.1 \leq q < 0.9$.

We randomly draw a value for the mass ratio for symmetric and asymmetric systems as defined above. Both of these mass ratio values are then assigned the same set of remaining input parameters required to calculate the orbital degradation factor. We then calculate and plot the distribution of the ratio of the orbital degradation factor for asymmetric systems to that for symmetric systems. The distribution obtained after 10^7 sample draws is shown in Fig. 3.

As we can see there are fewer systems in which the ratio has a value less than one, implying that the or-

bital degradation factor for asymmetric DNS systems is on average greater than that for a symmetric DNS systems. Consequently, asymmetric DNS systems are easier to detect in surveys as compared to symmetric DNS systems. However, despite the preference for the detection of asymmetric mass DNS systems, only two such systems have been detected, J0453+1559 ($q =$ Martinez et al. 2015) and J1913+1102 ($q = 0.75$ Ferdman et al. 2020), compared to eighteen other DNS systems with mass ratios $q \gtrsim 0.9$. This result suggests that this discrepancy in the number of detected asymmetric systems might not be due to selection effects, but rather due to differences in the evolutionary scenarios between the two types of systems.

3. ULTRA-COMPACT BINARY POPULATION STATISTICS

3.1. Size of population

Given the non-detection of UCB systems by current radio pulsar surveys, we can place an upper limit on the number of these systems in the Galaxy. To do so, we use the version of PSRPOPpy (Bates et al. 2014) that is integrated with the orbital degradation factor described in Sec. 2.4. We compute separately the upper limit on the population of ultra-compact NS–WD and DNS systems.

We follow a procedure that is based on the framework described in Kim et al. (2003). For any given type of binary system, if N_{obs} is the number of observed systems, we expect its probability distribution to follow a Poisson distribution:

$$P(N_{\text{obs}}; \lambda) = \frac{\lambda^{N_{\text{obs}}} e^{-\lambda}}{N_{\text{obs}}!} \quad (3)$$

where, by definition, $\lambda = \langle N_{\text{obs}} \rangle$. As described in Kim et al. (2003), we know that the relation

$$\lambda = \alpha N_{\text{tot}} \quad (4)$$

TABLE 2

THIS TABLE LISTS THE TELESCOPE AND SURVEY PARAMETERS FOR THE LARGE PULSAR SURVEYS THAT ARE CONSIDERED IN THIS WORK.

Survey –	Gain, G (K/Jy)	Center Frequency, f_c (MHz)	Bandwidth, B (MHz)	System temperature, T_{sys} (K)	Integration time, t_{int} (s)
PALFA ^a	8.5	1374	300	25	268
PMSURV ^b	0.6	1374	288	25	2100
AODRIFT ^c	10	327	25	100	50
GBNCC ^d	2	350	100	46	120
HTRU-low ^e	0.6	1352	340	25	340
HTRU-mid ^f	0.6	1352	340	25	540

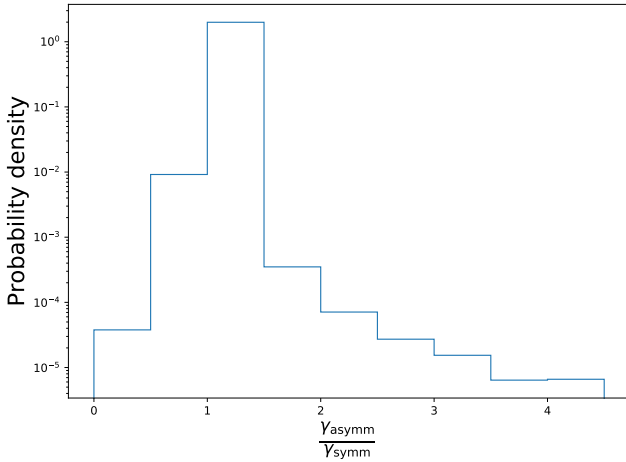
^aPulsar Arecibo L-band Feed Array, Cordes et al. (2006)^bParkes Multibeam SURvey, Manchester et al. (2001)^cArecibo DRIFT scan survey, Foster et al. (1995)^dGreen Bank North Celestial Cap Survey, Stovall et al. (2014)^eHigh Time Resolution Universe low-latitude survey Keith et al. (2010)^fHigh Time Resolution Universe mid-latitude survey Keith et al. (2010)

FIG. 3.— The ratio of the degradation factor for asymmetric mass systems to that of symmetric mass systems. The mass of the pulsar and all other orbital parameters, except the mass of the companion, are the same between the symmetric and asymmetric systems. The mass of the companion is calculated using the mass ratio, q , where for symmetric mass systems, $q \geq 0.9$ while for asymmetric mass systems, $q < 0.9$. The histogram shows that it is easier to detect asymmetric mass systems than symmetric mass systems.

is true, where N_{tot} is the number of UCB pulsars that are beaming towards the Earth and α is a constant that depends on the properties of the UCB system and the pulsar surveys under consideration. Since no UCB systems have been detected, we can set $N_{\text{obs}} = 0$, which reduces Eq. 3 to $P(0; \lambda) = e^{-\lambda}$.

As described in Kim et al. (2003), the likelihood function, $P(D|HX)$, where $D = 0$ is the real observed sample, H is our model hypothesis (i.e. Eq 4), and X is the population model, is defined as,

$$P(D|HX) = P(0|\lambda(N_{\text{tot}}), X) = e^{-\lambda(N_{\text{tot}})}. \quad (5)$$

Using Bayes' theorem and the justification given in Kim et al. (2003), the posterior, $P(\lambda|DX)$, is equal to the likelihood function, i.e.,

$$P(\lambda|DX) \equiv P(\lambda) = P(0|\lambda, X) = e^{-\lambda(N_{\text{tot}})}. \quad (6)$$

Using this posterior, we can calculate the probability distribution for N_{tot} ,

$$P(N_{\text{tot}}) = P(\lambda) \left| \frac{d\lambda}{dN_{\text{tot}}} \right| = \alpha e^{-\alpha N_{\text{tot}}}. \quad (7)$$

With PSRPOPpy, we generate populations of different sizes and calculate λ for each population using Eq. 3, which in combination with Eq. 4, gives us the value of α . Using Eq. 7 with the value of α gives us the probability density for the population of the UCB systems that are beaming towards Earth.

For all UCB systems, we allow the mass of the pulsar, m_1 , inclination of the system, i , the angle of periastron passage, ω_p , and the eccentricity, e , to have the range listed in Table 1. For ultra-compact NS-WD systems, we restrict the companion mass to the range $0.2 M_{\odot} < m_2 < 1.4 M_{\odot}$, while for ultra-compact DNS systems, we restrict the companion mass to the range $1.0 M_{\odot} < m_2 < 2.4 M_{\odot}$. We also assume the pulsar is an orthogonal rotator and thus, most of the power from the pulsar emission is constrained in the second harmonic, and set $m = 2$. In the case that the pulsar is not an orthogonal rotator, a choice of $m = 2$ results in a more conservative upper limit. For both ultra-compact NS-WD and DNS systems, we constrain the orbital period to the range 1.5 minutes $< P_b < 15$ minutes. All of these parameters have uniform distributions.

In addition, we constrain the spin period for DNS systems to the range 1 ms $< P_s < 100$ ms to correspond to the observed spin periods distribution and for NS-WD systems we assume a log-normal period distribution with mean and standard deviation of 4.5 ms and 1.8 ms respectively (Lorimer et al. 2015). We model the pulsar luminosity distribution using a log-normal distribution with a mean $\langle \log_{10} L \rangle = -1.1$ ($L = 0.07$ mJy kpc²) and standard deviation $\sigma_{\log_{10} L} = 0.9$ (Faucher-Giguère & Kaspi 2006). Since we consider surveys at different radio frequencies, we also model the pulsar spectral index as a normal distribution with mean $\alpha = -1.4$ and standard deviation $\beta = 1$ (Bates et al. 2013). We assume the radial distribution for the UCB systems as described in Lorimer et al. (2006) and the two-sided exponential function for the z -height distribution, with a scale height of $z_0 = 0.33$ kpc.

Finally, the surveys that we consider are listed in Table 2. These are the largest radio pulsar surveys conducted to date. The integration times from the individual surveys are used in the calculation of the orbital degradation factor. Using these parameters, the probability distribution for the size of the population of the UCB systems that are beaming towards the Earth is shown in Fig. 4. As we can see, the 95% upper limit

on the number of ultra-compact NS–WD systems in the Galaxy is 1450 systems, while that for ultra-compact DNS systems in the Galaxy is 1100 systems.

As stated earlier, the upper limits above are the number of UCB systems that are beaming towards Earth. The total number of these systems in the Galaxy can be calculated by scaling N_{tot} by the beaming correction factor, f_b (Kim et al. 2003). Given the large uncertainty in the beaming correction factors, if we use the average beaming correction factor measured for the merging DNS systems, $f_b = 4.6$ (Pol et al. 2019), the upper limit on the total number of ultra-compact NS–WD and DNS systems comes out to ~ 6700 and ~ 5000 systems respectively.

The number of ultra-compact DNS systems derived here is less than the total number of merging DNS systems derived in Pol et al. (2019) and Ferdman et al. (2020). This difference can be explained by the fact that the UCB systems that we consider in this work have lifetimes \sim few Myr, significantly smaller than that for the merging DNS systems studied in the aforementioned studies. As a result, these systems are closer to merger and spend a relatively short amount of time in this subclass of DNS systems compared to the larger orbital period merging DNS systems from Pol et al. (2019), which results in an overall smaller population size of ultra-compact DNS systems. The upper limit on the number of ultra-compact DNS systems is also consistent with recent estimates of the size of this population made by Lau et al. (2020) and Andrews et al. (2020). Note that in these simulations, we assumed that the luminosity function for both of these types of systems is the same and is the same as that of the observed pulsar population (Faucher-Giguère & Kaspi 2006). However, if the luminosity function for these systems is different, that will also influence the number of such systems in the galaxy.

3.2. Probability of pulsar surveys detecting an UCB system

Knowing the upper limit on the number of UCB systems that are beaming towards us, we can calculate the probability of the radio pulsar surveys listed in Table 2 in detecting these systems. To do so, we assume that the number of the UCB systems (both NS–WD and DNS) in the Galaxy is equal to their upper limits, i.e. we calculate the probability for these surveys in the most optimistic scenario.

Next, we use PSRPOPpy to generate this number of pulsars in the Galaxy, with the orbital, spin, luminosity, spatial and spectral index distributions being the same as described in Sec. 3.1. We generate 10^3 different versions of these populations to ensure that we are efficiently sampling all of the prior distributions. Accounting for the orbital degradation factor, we then “run” each of the surveys listed in Table 2 on each of these populations and count the number of systems that are detected by each survey. We then calculate the complementary cumulative distribution function for the number of detections by each survey, which is shown in Fig. 5.

As we can see, the surveys with the Arecibo radio telescope, i.e. PALFA and AODRIFT, have the highest probability to detect ≥ 1 of these UCB systems. This is followed by the GBNCC and HTRU mid-latitude survey, while the HTRU low-latitude and PMSURV have the least probability of detecting any of these UCB sys-

tems.

The difference in the efficiency of these surveys at detecting the UCB systems is due to the integration times used for processing these surveys. As can be seen in Table 2, AODRIFT has the shortest integration time of all the surveys, followed by GBNCC, PALFA, and the HTRU mid-latitude survey. A shorter integration time always produces a larger degradation factor, thereby providing a larger S/N detection for these systems.

However, it is possible to use a longer integration time and still maintain sensitivity to UCB systems, as is demonstrated by the PALFA survey. While the PALFA survey has the third-shortest integration time in Table 2, it is able to offset the relative loss in S/N due to the orbital degradation by increasing the overall sensitivity of the radio telescope. We discuss the balancing of the survey integration time with the orbital degradation factor further in Sec. 4.

3.3. Multi-messenger prospects for detectable ultra-compact binaries

In this optimistic scenario where the number of UCB systems beaming towards the Earth corresponds to the 95% upper limit derived above, we can expect to detect as many as four of these UCB systems with the radio pulsar surveys at Arecibo alone. Given their short orbital periods, these UCB systems could be promising sources for LISA, the space-based gravitational wave observatory that is scheduled to launch in the 2030s (Amaro-Seoane et al. 2017). To see if these systems will be detectable with LISA, we need to compute the S/N for these systems with respect to LISA’s sensitivity curve (Robson et al. 2019).

For a binary system with eccentricity, e , the GW emission from the system is spread over multiple harmonics of the orbital frequency, $f_n = n/P_b$, where n represents the n ’th harmonic. The total S/N for these systems as observed by LISA can be calculated as the quadrature sum of the S/N at each of these harmonics (D’Orazio & Samsing 2018; Kremer et al. 2018),

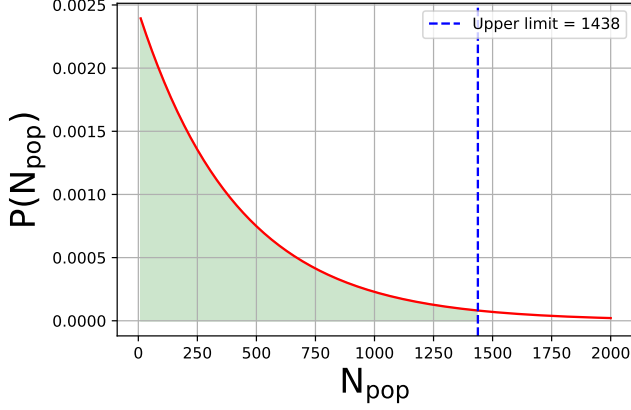
$$S/N^2 \approx \sum_{n=1}^{\infty} \frac{h_n^2(f_n) T_{\text{LISA}}}{S_{\text{LISA}}(f_n)} \quad (8)$$

where $S_{\text{LISA}}(f_n)$ is the LISA sensitivity curve as defined by Robson et al. (2019), $T_{\text{LISA}} = 4$ yrs is the timespan of the LISA mission, and $h_n(f_n)$ is the strain amplitude,

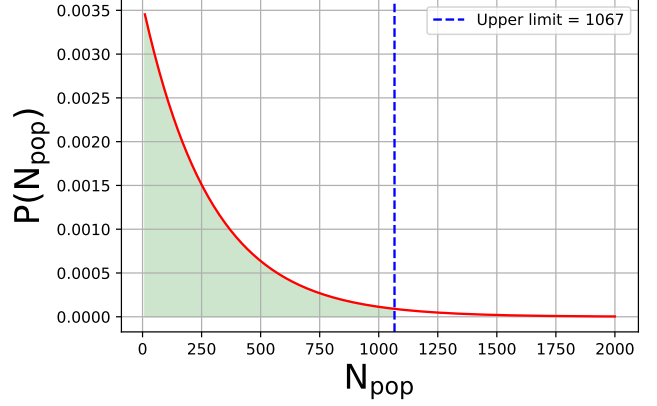
$$h_n(f_n) = \frac{8}{\sqrt{5}} \left(\frac{2}{n} \right)^{5/3} \frac{(\pi f_n)^{2/3} (\mathcal{G}\mathcal{M})^{5/3}}{c^4 d} \sqrt{g(n, e)} \quad (9)$$

where \mathcal{G} is the Gravitational constant, c is the speed of light, d is the distance to the binary system, $\mathcal{M} = m_1^{3/5} m_2^{3/5} (m_1 + m_2)^{-1/5}$ is the chirp mass of the binary, and $g(n, e)$ provides the relative amplitude between the different harmonics (see Eq. 20 in Peters & Mathews 1963).

Using these relations, we can calculate the S/N with which LISA would observe the UCB systems that are detected with the radio pulsar surveys described above. For the UCB binaries that were detected in the simulations described in Sec. 3.2 (both NS–WD and DNS), we extract the mass, m_1 and m_2 , of the components of the

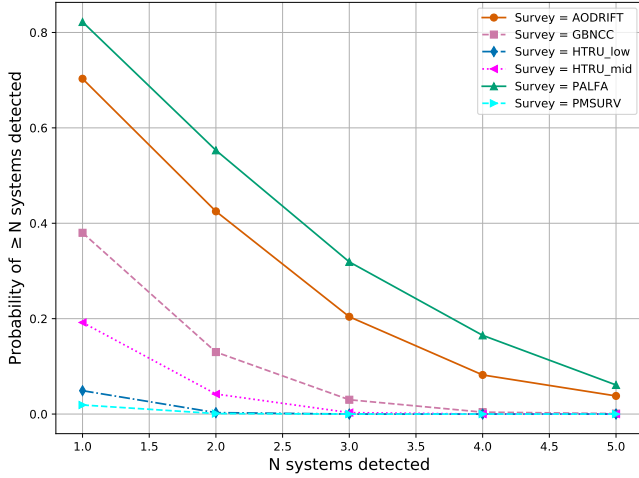


(a)

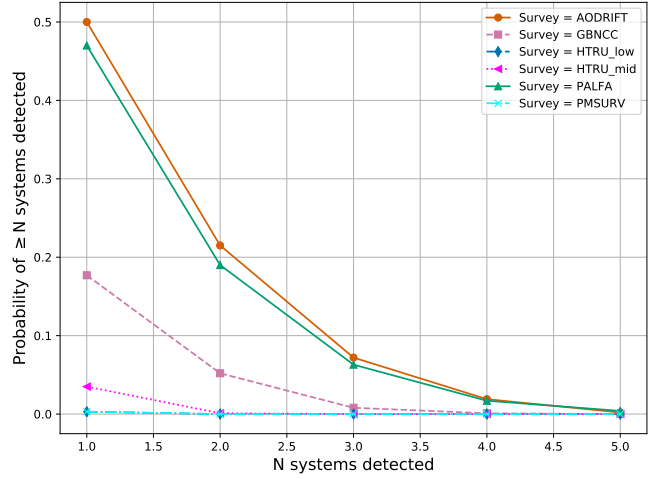


(b)

FIG. 4.— Probability distribution function for the number of UCB systems that are beaming towards the Earth. As we can see, the 95% upper limit on the number of ultra-compact NS-WD systems (panel (a)) is 1450 systems, while that for ultra-compact DNS systems (panel (b)) is 1100 systems.



(a)



(b)

FIG. 5.— Complementary cumulative distribution function of the number of UCB systems that are detectable by the radio pulsar surveys listed in Table 2. The X-axis shows the number of detected systems, N , while the Y-axis shows the probability that $\geq N$ systems will be detected in the given survey. The surveys conducted with the Arecibo telescope, i.e. PALFA and AODRIFT, are most likely to detect at least one of these UCB systems.

UCB system, the orbital period, P_b , eccentricity, e , and radial distance to the UCB system, d . We remind the reader that the radial distribution of the pulsars in the Galaxy was assumed to be the one described in Lorimer et al. (2006), while the z -height distribution was the one described in Lyne (1998). Given these parameters, we calculate the strain using Eq. 9 at harmonics $2 \leq n \leq 30$ and then calculate the S/N for each system by summing over these harmonics as described in Eq. 8.

All of the UCB systems that were detected in the radio pulsar surveys have an S/N that is comfortably above the LISA threshold $S/N = 7$ assuming a four year LISA mission. Thus, as shown in Sec. 3.2, even if radio pulsar surveys are able to detect only a couple of these UCB systems, these should be strong detections for LISA and will allow for multi-messenger studies of neutron stars (for example, see Thrane et al. 2020).

4. OPTIMUM INTEGRATION TIME FOR DETECTING ULTRA-COMPACT BNS SYSTEMS

As stated earlier, the impact of the orbital motion of the pulsar on the S/N is most acutely felt when the pulsar is part of an ultra-compact binary system (UCB). The modified radiometer equation for pulsars, including the orbital degradation factor, γ , can be written as (Lorimer & Kramer 2004):

$$S/N = \left[\frac{G\sqrt{BN_p}}{T_{\text{sys}}} \right] S \left[\sqrt{\frac{t_{\text{int}}(P_s - w)}{w}} \right] \gamma(t_{\text{int}}, P_s, \dots)^2 \\ = \xi \times S \times f_1(t_{\text{int}}, P_s, w) \times \gamma(t_{\text{int}}, P_s, \dots)^2 \quad (10)$$

where S is the pulsar flux, ξ is a constant that depends on the telescope and survey setup such as G , the receiver gain, B , the receiver bandwidth, $N_p = 2$, the number

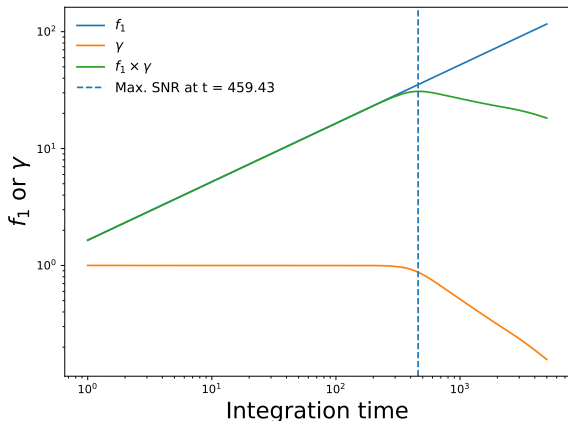


FIG. 6.— An example of maximizing the S/N by optimizing the selection of the integration time for the pulsar survey. This example uses the spin and orbital parameters of J0737–3039A (Double Pulsar, Burgay et al. 2005). The function, f_1 (Eq. 10), is directly proportional to the integration time, while there is a “knee” in the orbital degradation factor. As a result, the maximum S/N for this pulsar would be at an integration time of $t_{\text{int}} = 459$ s.

of polarizations, T_{sys} , the receiver system temperature (which includes the sky temperature, T_{sky}), P_s is the spin period of the pulsar and w is the effective pulse width (which includes effects of dispersion smearing and scattering). We list the telescope and survey parameters, as well as the integration times for the large pulsar surveys that we analyze in this work in Table 2.

For a pulsar with flux, S , we need to select an integration time, t_{int} , that maximizes the observed S/N for the pulsar in the BNS system. To motivate the problem, we show in Fig. 6 an example for a system that has the orbital and spin properties of the millisecond pulsar in the Double Pulsar system (Lyne et al. 2004; Burgay et al. 2005). As we can see, when the orbital degradation factor is not considered in the S/N calculation, the S/N for the system grows as a function of the integration time, $S/N \propto \sqrt{t_{\text{int}}}$. However, the orbital degradation factor function for this system has a “knee” at an integration time of ~ 460 s, after which the orbital degradation factor decreases with increasing integration time. As a result of this “knee” feature, the total S/N for the system peaks at the position of the “knee” introduced by the orbital degradation factor. Thus, the integration time corresponding to this peak would be the optimum integration time to detect systems like the Double Pulsar. Similarly, each binary pulsar system will have its own unique optimum integration time.

Note that ξ from Eq. 10 does not affect the optimum integration time, but will affect the final S/N of the system. This factor encodes the instrumental sensitivity of the telescope that is used for a given pulsar survey and thus, this factor will be larger for a more sensitive telescope. For example, for the PALFA survey at Arecibo, $\xi = 8.33$, while for the GBNCC survey at the Green Bank Telescope, $\xi = 0.61$. In fact, PALFA has the largest ξ value for any survey listed in Table 2, which explains why it has a high probability of detecting an UCB system despite having the third-shortest integration time (see Sec. 3.2). Despite this, it is still important to de-

rive and use an optimum integration time to maximize the probability of detecting an UCB system with all the surveys.

To generalize the example described above, we use a Monte Carlo simulation similar to the one described in Sec. 2.5. Since we are interested in UCB systems, we constrain the mass of the companion and the orbital period to the range $0.2 M_{\odot} < m_2 < 2.4 M_{\odot}$ and $1.5 \text{ min} < P_b < 15 \text{ min}$. In this case, as we desire simply a range of optimal integration times, we sample a uniform distribution of spin periods in the range 1 to 100 ms and assume a fixed duty cycle of $\delta = 0.06$ (Lorimer & Kramer 2004) and fix the harmonic to $m = 2$ (see Sec. 3.1). The other parameters have the same range as listed in Table 1. We draw 10^7 random samples from these distributions and calculate the optimum integration time as described above for each UCB system.

The above analysis yields an optimum integration time of $t_{\text{opt}} = 42^{+153}_{-22}$ s, where the errors represent the 95% confidence intervals on the peak of the distribution. Comparing this time to the integration times used for the large pulsar surveys in Table 2, we can see that the AODRIFT and GBNCC surveys are ideally placed towards detecting UCB systems, while PALFA is able to compensate for the loss in S/N by having a high ξ value as described above. This is also seen in Fig. 5, where these three surveys have the highest probability of detecting at least one UCB system.

Choosing an integration time from the range described above also leads to an average increase in the radiometer S/N, with the biggest effect seen for surveys whose integration times are much higher than the range derived above. For example, for the PALFA survey, reducing the integration time from 268 s to 50 s increases the S/N of the UCB systems by an average factor of 2.3. On the other hand, for PMSURV, which has the largest integration time of 2100 s, the S/N increases by an average factor of 4.5. The effect of this reduction in the integration time and increase in the S/N on the probability of detecting UCBs is shown in Fig. 7, where we can see a significant increase in the detection probability for the HTRU and PMSURV surveys.

However, given the relatively large range of the optimum survey integration times and the fact that each binary system will have its own optimum integration time, rather than picking a single integration time, we recommend implementing the “time domain resampling” technique (Johnston & Kulkarni 1991b; Ng et al. 2015). In this method, the integration time for a given survey is progressively reduced by a factor of 2 and each chunk of data is searched individually for binary systems. Using this method and starting with their design integration times, the survey will be most sensitive to UCB systems when the integration times are between 20 s and 200 s, which correspond approximately to the 95% confidence limits on the optimum integration time derived above. The “time domain resampling” method was most recently used in the HTRU survey (Ng et al. 2015), but only up to a minimum integration time of ~ 537 s, which optimized their search to binaries with orbital periods $P_b \geq 1.5$ hours. This led to the discovery of J1757–1854, which has an eccentricity, $e = 0.61$ orbital period of $P_b = 4.4$ hours and is the most eccentric DNS sys-

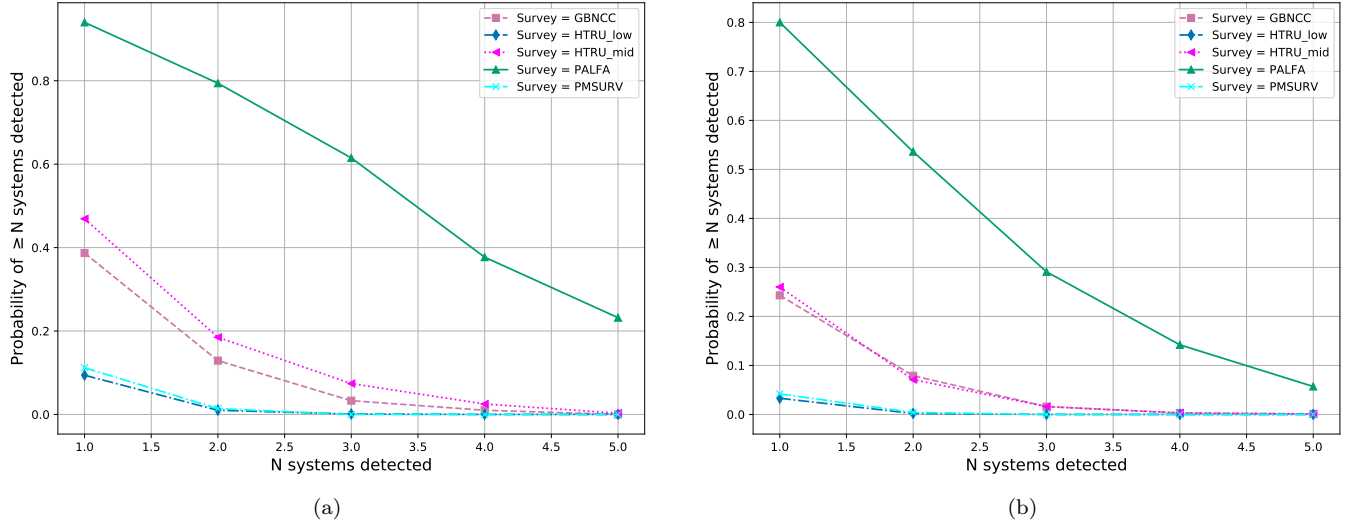


FIG. 7.— Complementary cumulative distribution function of the number of UCB systems that are detectable by the radio pulsar surveys listed in Table 2, but with integration time set to the optimum value of ~ 50 s derived in Sec. 4. The X-axis shows the number of detectable systems, N , while the Y-axis shows the probability that $\geq N$ systems will be detected in the given survey. Compared to Fig. 5, we can see a significant improvement in the detection probability for all the surveys.

tem detected (Cameron et al. 2018). Implementing the same time domain resampling technique on all surveys (except AODRIFT, due to its already low integration time) should increase the sensitivity of all the surveys to these UCB systems.

5. CONCLUSION

Using the framework developed by Bagchi et al. (2013), we develop a neural network to calculate the orbital degradation factor for any given binary system. We combine this neural network with PSRPOPpy opening the possibility for modeling the observed binary pulsar population. We show that, on average, it is easier to detect binary systems which are asymmetric in mass as compared to systems which are symmetric in mass.

We also investigate the population of UCB systems in the Milky Way as these systems are promising targets for the future space-based gravitational wave observatory LISA. We place upper limits of 1450 and 1100 ultra-compact NS-WD and DNS systems beaming towards the Earth respectively. We also show that the ra-

dio pulsar surveys with the Arecibo radio telescope have the highest probability of detecting at least one UCB system. Finally, we show that a survey integration time of $t_{\text{opt}} = 42^{+153}_{-22}$ s will maximize the S/N of the UCB systems.

Given the results this work, especially in Sec. 4, we strongly recommend reprocessing the data collected by the different radio pulsar surveys using the optimum integration time that we derive in this work. The optimum integration times should also be adopted by upcoming radio pulsar surveys at the MeerKAT (Sanidas et al. 2018; Bailes et al. 2020) and FAST (Nan et al. 2011) radio telescopes. Since the radio pulsar surveys conducted at these telescopes are potentially more sensitive than the Arecibo radio pulsar surveys analyzed in this work, they would have a correspondingly higher probability of detecting an UCB system.

NP and MAM are members of the NANOGrav Physics Frontiers Center (NSF PHY-1430284). MAM and DRL have additional support from NSF OIA-1458952 and DRL acknowledges support from the Research Corporation for Scientific Advancement and NSF AAG-1616042.

REFERENCES

- Abadi, M., Agarwal, A., Barham, P., et al. 2015, TensorFlow: Large-Scale Machine Learning on Heterogeneous Systems. <https://www.tensorflow.org/>
- Abbott, B. P., Abbott, R., Abbott, T. D., et al. 2017a, Physical Review Letters, 119, 161101, doi: 10.1103/PhysRevLett.119.161101
- . 2017b, ApJ, 848, L12, doi: 10.3847/2041-8213/aa91c9
- . 2020, ApJ, 892, L3, doi: 10.3847/2041-8213/ab75f5
- Accadia, T., Acernese, F., Alshourbagy, M., et al. 2012, Journal of Instrumentation, 7, 3012, doi: 10.1088/1748-0221/7/03/P03012
- Amaro-Seoane, P., Audley, H., Babak, S., et al. 2017, arXiv e-prints, arXiv:1702.00786. <https://arxiv.org/abs/1702.00786>
- Andersen, B. C., & Ransom, S. M. 2018, ApJ, 863, L13, doi: 10.3847/2041-8213/aad59f
- Andrews, J. J., Breivik, K., Pankow, C., D’Orazio, D. J., & Safarzadeh, M. 2020, ApJ, 892, L9, doi: 10.3847/2041-8213/ab5b9a
- Bagchi, M., Lorimer, D. R., & Wolfe, S. 2013, MNRAS, 432, 1303, doi: 10.1093/mnras/stt559
- Bailes, M., Jameson, A., Abbate, F., et al. 2020, PASA, 37, e028, doi: 10.1017/pasa.2020.19
- Bates, S. D., Lorimer, D. R., Rane, A., & Swiggum, J. 2014, MNRAS, 439, 2893, doi: 10.1093/mnras/stu157
- Bates, S. D., Lorimer, D. R., & Verbiest, J. P. W. 2013, MNRAS, 431, 1352, doi: 10.1093/mnras/stt257
- Brown, W. R., Kilic, M., Allende Prieto, C., & Kenyon, S. J. 2010, ApJ, 723, 1072, doi: 10.1088/0004-637X/723/2/1072
- Burgay, M., D’Amico, N., Possenti, A., et al. 2005, in Astronomical Society of the Pacific Conference Series, Vol. 328, Binary Radio Pulsars, ed. F. A. Rasio & I. H. Stairs, 53
- Cameron, A. D., Champion, D. J., Kramer, M., et al. 2018, MNRAS, 475, L57, doi: 10.1093/mnras/1/sly003
- Chollet, F., et al. 2015, Keras, <https://keras.io>
- Cordes, J. M., Freire, P. C. C., Lorimer, D. R., et al. 2006, ApJ, 637, 446, doi: 10.1086/498335
- D’Orazio, D. J., & Samsing, J. 2018, MNRAS, 481, 4775, doi: 10.1093/mnras/sty2568
- Eatough, R. P., Kramer, M., Lyne, A. G., & Keith, M. J. 2013, MNRAS, 431, 292, doi: 10.1093/mnras/stt161

- Faucher-Giguère, C.-A., & Kaspi, V. M. 2006, *ApJ*, 643, 332, doi: 10.1086/501516
- Ferdman, R. D., Freire, P. C. C., Perera, B. B. P., et al. 2020, *Nature*, 583, 211, doi: 10.1038/s41586-020-2439-x
- Foster, R. S., Cadwell, B. J., Wolszczan, A., & Anderson, S. B. 1995, *ApJ*, 454, 826, doi: 10.1086/176535
- Harry, G. M., & LIGO Scientific Collaboration. 2010, *Classical and Quantum Gravity*, 27, 084006, doi: 10.1088/0264-9381/27/8/084006
- Hessels, J. W. T., Ransom, S. M., Stairs, I. H., Kaspi, V. M., & Freire, P. C. C. 2007, *ApJ*, 670, 363, doi: 10.1086/521780
- Johnston, H. M., & Kulkarni, S. R. 1991a, *ApJ*, 368, 504, doi: 10.1086/169715
- . 1991b, *ApJ*, 368, 504, doi: 10.1086/169715
- Keith, M. J., Jameson, A., van Straten, W., et al. 2010, *MNRAS*, 409, 619, doi: 10.1111/j.1365-2966.2010.17325.x
- Kilic, M., Brown, W. R., Allende Prieto, C., Kenyon, S. J., & Panei, J. A. 2010, *ApJ*, 716, 122, doi: 10.1088/0004-637X/716/1/122
- Kim, C., Kalogera, V., & Lorimer, D. R. 2003, *ApJ*, 584, 985, doi: 10.1086/345740
- Kingma, D. P., & Ba, J. 2014, *arXiv e-prints*, arXiv:1412.6980. <https://arxiv.org/abs/1412.6980>
- Kremer, K., Chatterjee, S., Breivik, K., et al. 2018, *Phys. Rev. Lett.*, 120, 191103, doi: 10.1103/PhysRevLett.120.191103
- Lau, M. Y. M., Mandel, I., Vigna-Gómez, A., et al. 2020, *MNRAS*, 492, 3061, doi: 10.1093/mnras/staa002
- Lorimer, D. R., & Kramer, M. 2004, *Handbook of Pulsar Astronomy*, Vol. 4
- Lorimer, D. R., Faulkner, A. J., Lyne, A. G., et al. 2006, *MNRAS*, 372, 777, doi: 10.1111/j.1365-2966.2006.10887.x
- Lorimer, D. R., Esposito, P., Manchester, R. N., et al. 2015, *MNRAS*, 450, 2185, doi: 10.1093/mnras/stv804
- Lyne, A. G. 1998, *Advances in Space Research*, 21, 149, doi: 10.1016/S0273-1177(97)00799-0
- Lyne, A. G., Burgay, M., Kramer, M., et al. 2004, *Science*, 303, 1153, doi: 10.1126/science.1094645
- Manchester, R. N., Hobbs, G. B., Teoh, A., & Hobbs, M. 2005, *AJ*, 129, 1993, doi: 10.1086/428488
- Manchester, R. N., Lyne, A. G., Camilo, F., et al. 2001, *MNRAS*, 328, 17, doi: 10.1046/j.1365-8711.2001.04751.x
- Martinez, J. G., Stovall, K., Freire, P. C. C., et al. 2015, *ApJ*, 812, 143, doi: 10.1088/0004-637X/812/2/143
- Nan, R., Li, D., Jin, C., et al. 2011, *International Journal of Modern Physics D*, 20, 989, doi: 10.1142/S0218271811019335
- Napiwotzki, R., Yungelson, L., Nelemans, G., et al. 2004, in *Astronomical Society of the Pacific Conference Series*, Vol. 318, *Spectroscopically and Spatially Resolving the Components of the Close Binary Stars*, ed. R. W. Hilditch, H. Hensberge, & K. Pavlovski, 402–410. <https://arxiv.org/abs/astro-ph/0403595>
- Nelemans, G., Portegies Zwart, S. F., Verbunt, F., & Yungelson, L. R. 2001a, *A&A*, 368, 939, doi: 10.1051/0004-6361:20010049
- Nelemans, G., Yungelson, L. R., Portegies Zwart, S. F., & Verbunt, F. 2001b, *A&A*, 365, 491, doi: 10.1051/0004-6361:20000147
- Ng, C., Champion, D. J., Bailes, M., et al. 2015, *MNRAS*, 450, 2922, doi: 10.1093/mnras/stv753
- Pallanca, C., Ransom, S. M., Ferraro, F. R., et al. 2014, *ApJ*, 795, 29, doi: 10.1088/0004-637X/795/1/29
- Peters, P., & Mathews, J. 1963, *Phys. Rev.*, 131, 435, doi: 10.1103/PhysRev.131.435
- Pol, N., McLaughlin, M., & Lorimer, D. R. 2019, *ApJ*, 870, 71, doi: 10.3847/1538-4357/aaf006
- Ramachandran, P., Zoph, B., & Le, Q. V. 2017, *arXiv e-prints*, arXiv:1710.05941. <https://arxiv.org/abs/1710.05941>
- Robson, T., Cornish, N. J., & Liu, C. 2019, *Classical and Quantum Gravity*, 36, 105011, doi: 10.1088/1361-6382/ab1101
- Sanidas, S., Caleb, M., Driessen, L., et al. 2018, in *Pulsar Astrophysics the Next Fifty Years*, ed. P. Weltevredre, B. B. P. Perera, L. L. Preston, & S. Sanidas, Vol. 337, 406–407, doi: 10.1017/S1743921317009310
- Shah, S., Nelemans, G., & van der Sluys, M. 2013, *A&A*, 553, A82, doi: 10.1051/0004-6361/201321123
- Shah, S., van der Sluys, M., & Nelemans, G. 2012, *A&A*, 544, A153, doi: 10.1051/0004-6361/201219309
- Stovall, K., Lynch, R. S., Ransom, S. M., et al. 2014, *ApJ*, 791, 67, doi: 10.1088/0004-637X/791/1/67
- Stovall, K., Freire, P. C. C., Chatterjee, S., et al. 2018, *ArXiv e-prints*. <https://arxiv.org/abs/1802.01707>
- Thrane, E., Osłowski, S., & Lasky, P. D. 2020, *MNRAS*, 493, 5408, doi: 10.1093/mnras/staa593